Methodology for sizing stand-alone hybrid systems: A case study of a traffic control system

Idoia San Martín, Alberto Berrueta, Pablo Sanchis, Alfredo Ursúa*

Institute of Smart Cities, Department of Electrical and Electronic Engineering, Public University of Navarre, Campus de Arrosadía, 31006 Pamplona, Spain

*Corresponding author. Tel.: +34 948169276; fax: +34 948169884

E-mail address: alfredo.ursua@unavarra.es

Abstract

This paper proposes a methodology for sizing stand-alone hybrid photovoltaic-wind power generation systems. This methodology makes it possible to optimise the overall performance of the stand-alone system components, based on the premise of guaranteeing the power supply throughout the useful life of the installation at a minimum cost. The sizing is performed in two stages. Firstly, the components of the wind and photovoltaic power generation subsystem are obtained and, secondly, the size of the storage subsystem is determined. For the storage subsystem sizing, account is taken of the variation in efficiency according to the operating point and also the deterioration of the subsystem due to aging and, therefore, the loss of available energy during the useful life of the installation. This methodology is applied to a stand-alone traffic control system located on a secondary road in the Autonomous Community of Valencia (Spain). This system comprises wind and photovoltaic power generation components, a lithium battery bank and various traffic management components. Finally, an analysis of the proposed sizing is made. Satisfactory results are obtained, showing how the proposed methodology makes it possible to optimise the sizing of stand-alone systems with regard to the size of its components, cost and operation.

Keywords: Stand-alone hybrid systems, Renewable Energy, Sizing, Lithium-ion Battery, modelling

1 Introduction

Renewable energy-based stand-alone systems make it possible to supply power to those places where there is no nearby power grid or the cost of extending the power line is too high. Moreover, this renewable energy generation helps to mitigate the environmental impact of conventional energy sources. However, due to the intermittency of renewable energy resources, stand-alone renewable systems are faced with the problem of guaranteeing a continuous power supply. In this respect, hybrid systems using two or more renewable energy sources offer greater reliability of supply, design flexibility and, in general, greater profitability. In this context, the photovoltaic-wind power systems may represent an excellent trade-off between reliability of supply and cost, while the use of both energy sources means that it is possible to reduce the dependency on storage subsystems [1–3].

The storage subsystem in stand-alone systems must be capable of supplying power whenever the energy generated is insufficient to meet demand. It must also comply with certain requirements with regard to its power capacity and capability. Power capacity is necessary in order to adapt to the seasonal variability of the renewable resource, such as reduced irradiance in winter or a reduction in wind speed in summer. With regard to power requirements, the storage subsystem must be able to deal with power fluctuations resulting from renewable generation (rapid variations in wind speed and in irradiance) and from consumption (load connection and disconnection). Although there are a whole range of storage technologies, such as hydrogen [4-7], supercapacitors [8, 9], flywheel [10], etc., batteries are the technology that offers the best relationship between power density and energy density for use in stand-alone renewable systems [11,12]. Traditionally the lead acid battery was the most common technology in stand-alone systems, due to its low cost compared to other battery types [13-17]. However, over the last few years, the decreasing price of lithium-ion batteries and their improved performance compared to lead acid batteries (useful life, energy density and power density, deep cycles, etc.) mean that lithium-ion batteries are now an extremely attractive option for stand-alone renewable systems [18].

In the literature, there have been numerous investigations into methodologies for the sizing of stand-alone hybrid systems. Conventional methods are based on balancing the energy generated and consumed by the system, requiring the availability of meteorological data in order to estimate the energy generated [2]. Analytical techniques are also used, based on probabilistic methods, graphical constraint or computing tools [19]. Other methods are based on advanced optimisation techniques with genetic algorithms, artificial neural networks or fuzzy logic [20-22]. Likewise, there are a number of commercially available software packages such as HOMER, HOGA and HYBRID2, which make it possible to perform the sizing of stand-alone systems [23]. In general, the sizing methods are based on reliability and/or economic criteria,

such as loss of power supply probability, cost per kWh, level of autonomy, total cost and load energy requirements or yearly loss of load probability [19, 20, 24]. In short, the sizing methods are directed at obtaining stand-alone systems that guarantee the energy supply and minimise installation costs. Some of these methodologies consider a constant storage subsystem efficiency for the sizing [12-16], whereas others consider an efficiency which varies according to the storage subsystem operating point (current and/or state of charge) [21, 23]. This makes it possible to obtain a sizing which is more in line with the application.

Traditionally, sizing methodologies have considered the useful life of the system components and the costs involved in replacing the equipment and its maintenance [25]. However, little attention has been paid to the problems presented by the deterioration of the storage subsystem. Generally, batteries are an essential part of stand-alone renewable systems as they ultimately guarantee a continuous power supply to the system loads during the expected useful life, and not solely during the first years of operation. Batteries degrade due to use and also over time. The principal causes of this degradation, known as aging, are related to time, charge processing and certain operating parameters such as temperature, state of charge, current and depth of discharge. A common approach is to distinguish between calendar aging (a consequence of the passage of time) and cycle aging (a consequence of the battery use) [26]. Battery aging results in capacity fade, on the one hand, meaning that less energy can be stored and, on the other hand, power fade, which is an increase in the internal resistance and subsequent reduction in the power management capability. With regard to the above, battery aging may mean that, at a given moment in time, there is insufficient power to supply the stand-alone systems loads. Moreover, to a large extent, the battery aging determines the useful life of the system. For both reasons, it is important to include the aging phenomenon in the stand-alone system sizing methodology. It is therefore possible to ensure a continuous power supply during the useful life of the corresponding stand-alone installation.

This paper develops a methodology for sizing stand-alone systems in order to optimise the sizing of all the system components, including the storage subsystem, based on the premise of meeting the energy requirements throughout the useful life of the installation at a minimum cost. Specifically, the proposed methodology is applied to a stand-alone traffic control system (TCS) located on a secondary road. This system comprises a wind and photovoltaic (PV) renewable energy generation subsystem, a battery-based energy storage sub-system and a TCS made up of a Universal Remote Station (URS), two Variable Message Signs (VMS) and a number of sensors (turn magnetics, laser sensors and fog sensors). Finally, an analysis of the proposed sizing is made and, in turn, this is compared with more conventional sizing methodologies. The methodology developed in this article can be applied to a wide range of

stand-alone systems and, specifically, it is extremely useful for those systems in which there must be a continuous power supply to the loads.

2 Description of the sizing methodology

This section provides a general description of the methodology for sizing stand-alone hybrid PV-wind systems. The ultimate aim is to optimise the renewable generation components and the storage subsystem, ensuring a continuous power supply to the loads throughout the useful life of the installation at a minimum cost.

Fig. 1 shows a flow diagram of the proposed methodology. The methodology is divided into two stages. The first stage involves the sizing of the generation components, while the storage subsystem sizing is determined in the second stage. The first stage determines the required number of wind-turbines (N_W) and PV modules (N_{PV}). Once the number of renewable energy generation components has been obtained, the next step is to size the storage subsystem, in other words the number of batteries required. This second stage is broken down into three steps: pre-sizing, sizing by electrical model and sizing by aging model. The first step, pre-sizing, gives the number of batteries required (N_{c_P}) considering the battery efficiency to be constant. The next step is the sizing by electrical model in order to obtain the number of batteries required (N_{c_EM}) considering a variable efficiency obtained through the battery electrical modelling. The third and final step is the sizing by aging model which makes it possible to obtain the number of batteries required in order to guarantee a continuous power supply to the stand-alone system loads (N_{c_AM}) throughout the useful life of the installation.

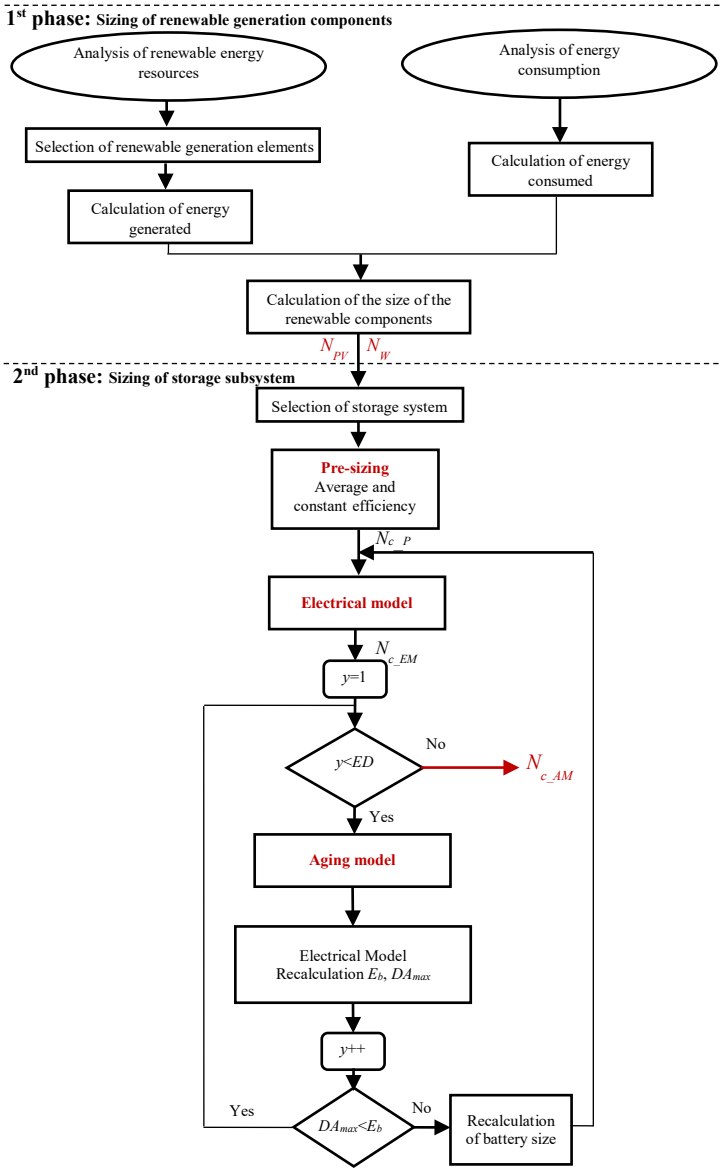

Fig. 1. Flow diagram of the proposed sizing methodology

2.1 Sizing of the renewable energy generation elements

2.1.1 Resource analysis

For the power supply system sizing, a study needs to be made of the energy resources (wind and solar) available at the installation site. The aim is to calculate the wind and PV hourly energy per area unit.

The available wind potential can be obtained from databases or companies specialising in obtaining the wind resource [27]. Generally, the baseline data used are the hourly wind speed at a given height for a typical year at the site. This height does not usually match that of the wind turbine hub and, therefore, in order to obtain wind speed (v) at wind turbine height (h) baseline speed (v_{ref}) is extrapolated to baseline height (h_{ref}) taking account of the ruggedness of the terrain (h_0) using the following expression:

$$v = v_{ref} \cdot \frac{\ln\left(h/h_0\right)}{\ln\left(h_{ref}/h_0\right)} \quad (1)$$

The calculation of the wind power generated is made using the power curve for the wind turbine selected, in relation to the wind speed. Furthermore, the power stage efficiency is taken into account. This efficiency varies between 92 to 98% depending on the electronic converter topology [28].

With regard to the solar resources, the data can also be obtained from databases or companies specialising in energy resources [29-31]. In general, this is based on daily radiation on a horizontal surface for a typical year, while temperature data are also available to better characterise the solar resource. The values for global radiation on a horizontal surface are used to obtain the beam and diffuse radiation on a horizontal surface. The next step is to determine the optimum PV module tilt, which depends on the latitude of the site, and it is south facing. This tilt is used to obtain the tilted surface radiation (beam, diffuse and reflected). And, taking a number of losses into account (incidence angle, soiling, temperature, mismatch losses) the PV energy is calculated [32, 33]. Furthermore, the power stage efficiency is taken into account. This efficiency varies between 95 to 98% depending on the electronic converter topology [27].

2.1.2 Consumption analysis

The installation consumption must be determined, in order to correctly apply the sizing methodology. To do so, this consumption can either be estimated or experimental measurements can be taken during a given system operating time. This consumption must include the efficiency of the conversion stage to supply the system loads. Furthermore, it is important to analyse the various system loads given the fact that, on occasions, it is possible to minimise their consumption and, therefore, to reduce the size of the stand-alone power system.

2.1.3 Sizing of the renewable generation subsystem

Once the renewable resource and the consumption of the stand-alone installation have been analysed and characterised, the next step is the sizing of the renewable generation components. To do so, firstly f is defined as the fraction of the energy consumption covered by the PV subsystem and (1-f) the fraction covered by the wind-power subsystem. Therefore, the energy balance of the renewable energy system can be expressed as follows:

$$e_{pv} \cdot A_{pv} = f \cdot E_{con} \quad (2)$$

$$e_w \cdot A_w = (1 - f) \cdot E_{con} \quad (3)$$

where e_{pv} and e_w represent the PV and wind energy generated per area unit, A_{pv} and A_w represent the area of the PV and wind-power subsystems respectively, and E_{con} is the energy consumed.

Parameter f varies from 0 to 1 with increments of 0.1. When $f = 0$, all the consumption is covered by the wind-power subsystem. Conversely, for $f = 1$, all the consumption is covered by the PV subsystem.

The method considers the worst month from an overall perspective, in other words, taking both energy resources into account. The selection of this month as a baseline for the sizing represents an intermediate solution between the use of a month with mean annual data and the independent calculation of each of the generation subsystems for their respective worst months. This is due to the fact that the use of a mean month with annual data would lead to an insufficient power supply system and the independent selection of the worse months for each resource would lead to an over-sized system [34]. Considering the worst month involves making the sizing for the month in which the total area, namely the sum of the PV and wind-power area, to cover consumption is at its maximum. Therefore, the areas for the generation subsystems for each month of year i, can be expressed as follows:

$$A_{pv,i} = f \cdot \frac{E_{con,i}}{e_{pv,i}} \tag{4}$$

$$A_{w,i} = (1 - f) \cdot \frac{E_{con,i}}{e_{w,i}} \tag{5}$$

$$A_i = A_{pv,i} + A_{w,i} \quad , i = 1,2,\ldots 12 \tag{6}$$

The areas for each generation subsystem can be used to calculate the installed power in each area. The month with the highest sum of both powers is termed the worst month.

Given the fact that the areas of the subsystems are dependent on f there is a worst month for each value of f. Therefore, the method will obtain 11 combinations of wind turbines and PV modules, which correspond to 11 possible values of f. The results obtained represent the exact areas required to cover consumption. The definitive number of wind turbines (N_w) and PV modules (N_{pv}) is the one that makes it possible to guarantee an area that is equal to or greater than the one calculated.

2.2 Sizing of the storage subsystem

2.2.1 Pre-sizing of the storage subsystem

The first stage of the storage subsystem sizing involves the pre-sizing of the battery bank considering a zero loss of load probability and therefore guaranteeing a continuous power supply. This pre-sizing is based on considering a mean and constant efficiency of the battery bank, regardless of its operating mode. For each value of f, the hourly energy difference ($D_{j,f}$) is calculated through the hourly energy generated ($E_{gen,j,f}$) and consumed ($E_{con,j}$):

$$D_{j,f} = E_{con,j} - E_{gen,j,f}\ , j = 1,2,\ldots 8760; f = 0,\ 0.1,\ldots 1 \tag{7}$$

where $E_{gen,j,f}$ is calculated as the sum of the hourly energy generated by each renewable subsystem:

$$E_{gen,j,f} = N_{w,f} \cdot A_{w,f} \cdot E_{w,j,f} + N_{pv,f} \cdot A_{pv,f} \cdot E_{pv,j,f}\ , j = 1,2,\ldots 8760; f = 0,0.1,\ldots 1 \tag{8}$$

The battery bank must cover the difference (D). If the difference is positive, then E_{con} is not completely covered by the renewable generation subsystem and the energy deficit must be supplied by the battery bank. Conversely, when E_{gen} is greater than E_{con}, the battery bank can store the excess energy. Calculated below is the cumulative energy difference (DA) for each hour of the year and for each f value, based on the DA for the previous hour and the D for the current hour, using the following expression:

$$DA_{j,f} = DA_{j-1,f} + \mathrm{C}_{c,d} \cdot D_{j,f}\ , j = 1,2,\ldots 8760; f = 0,\ 0.1,\ldots 1 \tag{9}$$

where $C_{c,d}$ is a coefficient which takes account of the battery bank charge or discharge efficiency and that of the dc/dc reversible converter. When D is positive, $C_{c,d}$ is equal to the inverse of the discharge efficiency, $C_{c,d} = 1/\eta_d$. This is due to the fact that, for the battery bank to provide this energy difference, it must store this difference plus the losses caused during the discharge process. On the contrary, when D is negative, $C_{d,c}$ is equal to the charge efficiency, that is $C_{d,c} = \eta_c$, given the fact that the energy stored is less than the energy input into the battery bank, due to the energy losses generated during the charging process. In order to calculate the DA the initial cumulative energy difference is considered to be zero ($DA_{0,f} = 0$). Given the fact that the purpose of the battery bank is not to store all the renewable energy generated but to cover demand when the energy resource is insufficient to do so, when DA_j is negative, it is imposed that $DA_{j,f} = 0$. This prevents the over-sizing of the battery bank. The maximum DA value over the year analysed provides the maximum cumulative difference ($DA_{max,f}$). This difference determines the size of the battery bank for the case in which the said battery bank must always cover the difference between generation and consumption.

The maximum battery bank Depth of Discharge (DOD_{max}) is used to obtain the number of batteries required for each value of f($N_{c\_P,f}$).

$$N_{c\_P,f} = \frac{DA_{\max,f}}{DOD_{\max} \cdot E_b}\ , f = 0,\ 0.1,\ldots 1 \tag{10}$$

where E_b is the energy of each battery cell obtained as the product of capacity (C_c) and the rated voltage of each cell (V_c):

$$E_b = C_c \cdot V_c \tag{11}$$

2.2.2 Sizing of the storage subsystem by electrical model

The second stage of the storage subsystem sizing is based on the use of the battery bank electrical model. This makes it possible to obtain a sizing that is more in line with the actual application, given the fact that its electrical performance varies according to the battery operating point. Depending on the battery technology used, the influence of efficiency on the operating point could be significant. This can be seen in lead acid batteries, in which efficiency drops considerably at state of charge (SOC) above 80%.

To perform this sizing stage, an electrical model representing the battery bank efficiency is required. Based on this, with the data for the power to be provided by the battery bank and the number of batteries obtained in the pre-sizing (N_{c_P}), the battery bank efficiency variation is calculated for each hour of the year. The next step is to apply Eqs. (9) and (10) in order to obtain the number of batteries required, in this case termed N_{c_EM}. This procedure is repeated for each value of f.

2.2.3 Sizing of storage subsystem by aging model

The third and final stage of the subsystem storage sizing is based on considering the aging of the same. As a battery ages, its capacity diminishes and its internal resistance increases. Therefore, the energy available gradually diminishes over the years, as does the energy conversion performance. In order to perform the sizing by taking aging into account, there is a need for an aging model that takes account of the processes that cause the battery to deteriorate. This aging model depends on the battery operating characteristics, such as the number of cycles, depth of discharge, charge and discharge currents, operating voltage, temperature, etc. It is therefore necessary to have an electrical model of the battery in order to determine the evolution of the state of charge, voltage and current in relation to the power absorbed or supplied by the battery.

As seen in Fig. 1, the data obtained in the sizing with the electrical model (N_{c_EM}) are used as a baseline, and the expected duration of the batteries is indicated in years (ED). The electrical model for the battery and the hourly power profile over a year of operation, to be covered by the batteries (D) gives the voltage, current and SOC for each hour of the year. These data are entered in the aging model to obtain the actual capacity (C_a) and actual internal resistance (R_a) of the battery after the first year of operation ($y = 1$). Then, the C_a and R_a values are used to recalculate DA_{max} and E_b through Eqs. (9-11). If the actual battery is able to cover the maximum difference ($DA_{max}<E_b$) then the following year is considered, provided that ED is greater than the year under study ($ED > y$). In turn, once the C_a and R_a values are obtained, then the C_a and R_a values for the year under study are calculated using the aging model DA_{max} and E_b through the electrical model. This procedure is adopted, provided that $DA_{max}<E_b$ is met and the year under study is less than ED. When $ED < y$, this marks the end of the iterative process and the C_a

value obtained is the required capacity for the battery. Moreover, if $DA_{max} < E_b$ is not met for a year, then the process is repeated from the start with the capacity obtained.

Finally, based on the C_a value obtained and with the data for each battery cell (C_c, V_c) the number of cells required (N_{c_AM}) is obtained, repeating this process for each value of f:

$$N_{c\_AM,f} = \frac{N_{c\_EM,f} \cdot C_{a,f} \cdot V_c}{C_c \cdot V_c} \quad , f = 0,\ 0.1, \ldots 1 \tag{12}$$

2.3 Selection of a solution

The proposed sizing methodology results in 11 possible solutions that meet the energy requirements. In other words, they guarantee the continuous supply of power to the load. Each of these 11 potential solutions has an associated financial cost. The optimal solution is the one involving the lowest cost for the stand-alone system. Account should be taken of the fact that, by applying the complete sizing methodology, in other words based on all three stages, the result obtained guarantees the continuous power supply to the loads throughout the useful life of the installation.

3 A case study: a traffic control stand-alone system

3.1 Description of the TCS

The majority of traffic accidents with loss of life occurring on interurban networks, take place on secondary or all-purpose roads. This can be seen on Spanish roads, where 75% of the accidents with loss of life in 2016 took place on secondary roads [35]. The use of TCS helps to reduce the accident rate [36, 37]. Generally these secondary roads are not equipped with TCS, primarily due to cost and to the difficulty of providing a power supply and communication system with the traffic control centres. The absence of a power grid close to these roads and the high cost involved in extending the power line, as a result of the great distances and the rough terrain, makes it necessary to develop stand-alone power systems, preferably based on renewable energy sources.

The methodology proposed in this paper is applied to a stand-alone TCS to be implemented on a secondary road. The work comes within the framework of research project: DPI2006-15703-C02-02. Specifically, the stand-alone TCS is located at kilometre 134 of secondary road CV-25 (see Fig. 2) which is part of the road network in the Autonomous Community of Valencia (Spain) and which comprises, as shown in Fig. 3, a wind and PV renewable energy generation subsystem, a battery-based energy storage subsystem and a TCS comprising a Universal Remote Station (URS), two variable Message Signs (VMS) and a number of sensors (turn magnetics, laser sensors and fog sensors). Fig. 4 shows a diagram of the TCS component parts.

The URS is responsible for communications with the traffic control centre and with the other TCS. The URS receives messages from the other TCS and acts accordingly, communicating with the traffic control centre and the VMS. On the other hand, the URS is able to warn the traffic control centre of any system failure, such as a fault in the renewable generation subsystem or in the storage subsystem. The URS is the critical load of the TCS and must not be cut off from the electricity supply.

Fig. 2. Photo (left) and map (right) of the TCS site [38] located at kilometre 134 on secondary road CV-25, forming part of the road network of the Autonomous Community of Valencia (Spain).

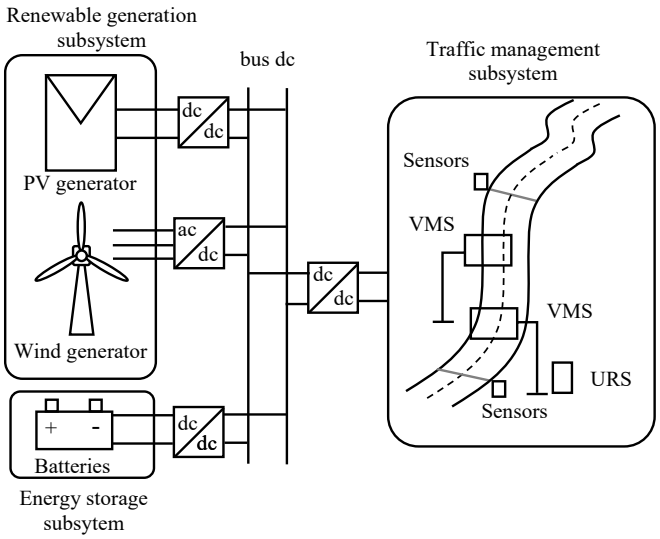

Fig. 3. Diagram of the stand-alone TCS.

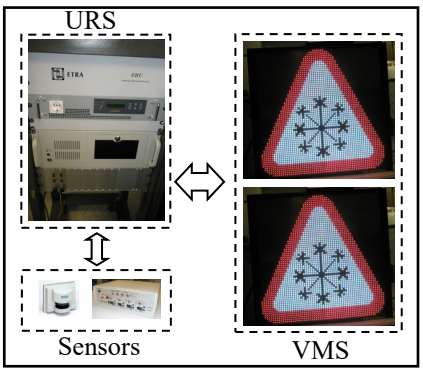

Fig. 4. Diagram of the components forming part of the TCS: URS, VMS and sensors.

3.2 Application of the TCS sizing methodology

3.2.1 Estimation of the energy consumed by the TCS

TCS have traditionally been designed to be connected to the power grid, consequently; they have achieved high functional characteristics with no energy restrictions. For this reason, from an energy consumption point of view, they suffer from shortcomings such as redundant conversion stages or over-sized power supplies. Current TCS have a low energy efficiency and, therefore, an analysis needs to be made in order to reduce their power consumption, thereby helping to reduce the cost of the stand-alone renewable system.

As described in Section 3, the TCS comprises two VMS, a URS and a number of sensors. In order to reduce consumption, the VMS are only activated by a vehicle passing by and remain on for 4 sec., which is considered to be sufficient time for the driver to receive the information. In order to obtain the consumption of the system, the power absorbed by each element was measured using a YOKOGAWA WT3000 data logger. The results obtained show that the consumption of each VMS is 300 W when all the LEDs are lit with the maximum brightness level, and 20 W in stand-by mode, that is when the LEDs are off. The URS consumes 78 W and the sensors 15 W. In short, the system comprises three loads with continuous consumption (the sensors, URS, and VMS stand-by mode) and an intermittent consumption load (the VMS activated as a vehicle passes by).

In order to estimate the electrical consumption associated with the intermittency of the VMS operation, the distribution of vehicles in the section of the road in which the system is located was used. Specifically, the data used correspond to the mean number of daily vehicle from 2012 to 2016 for each month of the year, differentiating between a working day, Saturday or Sunday, as shown in Fig. 5 a [38]. Furthermore, the hourly distribution of the number of vehicles over a typical day was used, as shown in Fig. 5 b. Taking the annual mean, the number of vehicles circulating in the course of the day is 1866, and the total consumption of the system in its original configuration is 3775.2 Wh per day.

On the other hand, in order to minimise the energy consumption of the conventional TCS, and to thereby reduce the renewable power supply system, the following three actions were taken:

i) Use of the VMS switch. This switch is used to cut-off the power supply to the LEDs in the absence of a vehicle.
ii) Removal of the three-phase power supply for each VMS. This makes it possible to avoid losses in the power supply.
iii) Removal of the uninterruptible power supply in the URS, given the fact that the actual power supply system performs like an UPS.

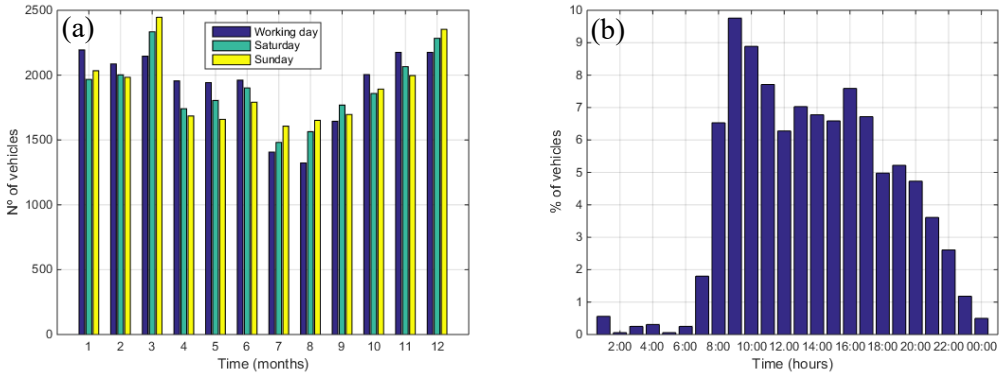

Fig. 5. a) Number of vehicles per day for each month on a working day, Saturday and Sunday and b) the hourly distribution of vehicles at kilometre 134 on secondary road CV-25, forming part of the road network of the Autonomous Community of Valencia (Spain).

Applying the three actions described above, a daily TCS consumption of 2133.1 Wh is obtained. This involves a reduction in daily consumption of 1642.1 Wh, and an energy saving of 43.5%. This energy saving entails a considerable reduction in the renewable energy generation subsystem and in the associated cost.

As shown in Fig. 3 the system loads are supplied through a non-reversible dc/dc converter. Therefore, an efficiency of 96% in the power stage is considered for the calculation of the energy consumed.

3.2.2 Estimation of the energy generated

The first step was to select the wind turbine and PV module for the hybrid power supply system. The wind turbine selected was the Silentwind 24 manufactured by the company SilentWind with a rated power of 450 W, a rotor diameter of 1.15 m and a tower of 15 m (height from the ground to the hub) [39], and the PV module selected was the E-75P polycrystalline model made by the company Ennova Energía with a peak power of 75 W and an area of 0.51 m^2 [40].

An analysis was made of the wind potential available at the site of the stand-alone TCS using the hourly data for the wind speed at a height of 10 metres, obtained from the company Meteosim Truewind S.L.[27]. Fig. 6 a shows the hourly wind potential for a typical year at the said site, with a wind speed at a height of 10 metres. In order to obtain the wind speed at the wind turbine height (h = 15 m) the baseline speed was extrapolated taking the roughness of the terrain into account (h_0 = 0.2 m) by Eq. (1). The calculation of the hourly wind power generated, as discussed in subsection 2.1.1, was performed using the power curve in relation to the wind speed of the Silentwind 24 wind turbine, provided by the manufacturer. Specifically, a sixth grade polynomial was constructed from the said curve, relating the wind power generated with the wind speed. Furthermore, a 94% efficiency was considered for the power stage, which is a non-reversible converter.

The solar resource of the stand-alone TCS site was obtained from the Atmospheric science data centre [29]. Daily global radiation and temperature data from 1984 to 2004 were used to create a typical year. To do so, the monthly mean for the 22 years was established, selecting the typical month as the one closest to the mean, thereby constructing a typical solar resource year. Fig. 6 b shows the hourly PV potential for a typical year at the said site, hourly average solar irradiation (kW m^{-2}). As mentioned in subsection 2.1.1, the global horizontal irradiance values are used to calculate the PV hourly power. To do so, the optimal panel tilt is determined: 31º (*degree tilted, south oriented*). Furthermore, a 96% efficiency was considered for the non-reversible power converter.

3.2.3 Sizing of the power generation components

Based on the data for the wind and PV hourly power output, the wind and PV monthly energy is calculated per area unit. Applying Eqs. (2) – (6) to obtain the wind and PV areas required to cover the consumption corresponding to the *worst month* for the different values of *f*. The areas required for wind power (A_w) and PV power (A_{pv}) and the definitive number of wind turbines (N_w) and PV modules (N_{pv}) for each value of *f* are shown in Table 1. It is worth noting that the proposed methodology calculates the areas required for each technology. In order to obtain the N_W and N_{PV} required, these values are recalculated so as to obtain the exact areas that can finally be installed and this depends on the basic unit of each element. In short, in order to select the basic generation units, a trade-off needs to be sought between a minimum and maximum in order to avoid too many units or to oversize the system, with the subsequent cost increase in both cases.

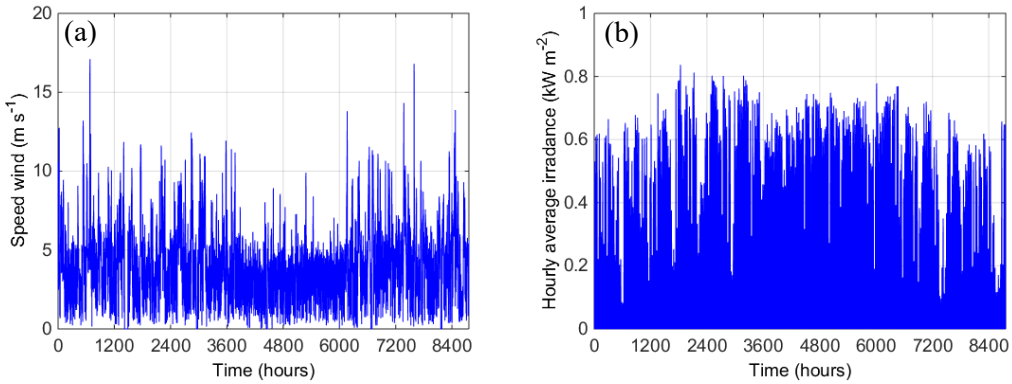

Fig. 6. Wind and PV power potential at the site of the stand-alone TCS: a) wind speed (m s^{-1}) and b) hourly average solar irradiance (kW m^{-2}).

f	A_w (m^2)	A_{pv} (m^2)	N_w	N_{pv}
0	2.94	0.00	3	0
0.1	2.65	0.31	3	1
0.2	2.36	0.62	3	2
0.3	1.05	1.98	1	4
0.4	0.90	2.64	1	6
0.5	0.75	3.30	1	7
0.6	0.60	3.96	1	8
0.7	0.45	4.62	1	10
0.8	0.30	5.27	1	11
0.9	0.15	5.93	1	12
1	0.00	6.59	0	13

Table 1. Sizing of generation elements.

3.2.4 Pre-sizing

The batteries selected for this system are commercial lithium-ion ones. Each cell has a capacity of 40 Ah and a voltage of 3.7 V, and has a carbon-black anode, an NMC cathode and an organic polymer electrolyte. These cells are punch type [41].

For each of the 11 solutions, the DA is obtained through Eqs. (7) and (9). For this purpose, a mean energy efficiency for the charging and discharging of the battery bank of 95% was considered and a battery bank reversible converter efficiency of 96%. That is η_c = 0.92 y η_d = 0.92. With DA_{max} and Eq. (10) is used to obtain the number of batteries for each value of f, in this case the batteries are named as $N_{c\_P.}$ For this purpose, a DOD_{max} of 100% was considered.

3.2.5 Sizing of the battery bank by electrical model

In order to perform the second stage of the subsystem storage sizing, an electrical model of the selected batteries is required. The electrical model used is based on the one presented by Berrueta [42], although adapted for a battery comprising a 40 Ah lithium-ion cell. Furthermore, the load transfer capacitor was disregarded, given that it does not affect the system sizing. The electrical model used is shown in Fig. 7, comprising a voltage source (V_{oc}) dependent on the SOC, and internal resistor (R) representing the ohmic resistance and the load transfer, and it is also a function of the SOC. Eqs. (13) and (14) show the expressions V_{oc} and R based on the SOC.

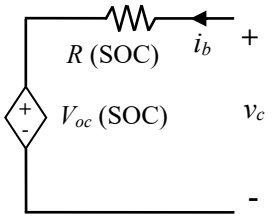

Fig. 7. Electrical model of a lithium-ion cell.

$$V_{oc} = -337.42 \cdot SOC^8 + 1520.4 \cdot SOC^7 - 2842.50 \cdot SOC^6 + 2846.70 \cdot SOC^5 - 1646.50 \cdot SOC^4 + \\ + 554.89 \cdot SOC^3 - 105.14 \cdot SOC^2 + 10.67 \cdot SOC + 3.05 \quad (13)$$

$$R = -30.74 \cdot SOC^8 + 124.40 \cdot SOC^7 - 209.40 \cdot SOC^6 + 188.90 \cdot SOC^5 - 97.69 \cdot SOC^4 + \\ + 28.38 \cdot SOC^3 - 4.15 \cdot SOC^2 + 0.22 \cdot SOC + 0.12 \quad (14)$$

where the actual SOC is calculated through current (i_b), cell capacity (C) and the previous SOC:

$$SOC = SOC_{i-1} + \frac{\int i_b \cdot dt}{C} \quad (15)$$

As detailed in subsection 2.2.2, for each of the 11 potential solutions, a calculation is made of the efficiency, η_b, of the battery bank through the electrical model for each hour of the year, considering the power to be supplied by the battery bank (D) and the number of batteries obtained in the pre-sizing (N_{c_P}).

$$\eta_b = 1 - \frac{R \cdot {i_b}^2}{|D|} \quad (16)$$

Based on this efficiency, the DA is obtained by applying Eq. (9) and the required number of batteries, N_{c_EM}, through Eq. (10).

3.2.6 Sizing of battery bank by aging model

In the final stage of the storage subsystem sizing, it is necessary to have an aging model for the batteries selected, representing the deterioration suffered over time and based on the battery operating mode.

The aging model used combines the effects of calendar aging and cycle aging and makes it possible to obtain the decrease in the battery capacity and the increase in its internal resistance. The effect of calendar aging has a linear dependence on time (t) while cycle aging has a linear dependence on equivalent cycles (Q). The reduction in capacity ($\Delta C/C$) and the increase in internal resistance ($\Delta R/R$) are modelled with the following expressions:

$$\frac{\Delta C}{C} = -\left(\alpha_c \cdot t + \beta_c \cdot Q\right) \quad (17)$$

$$\frac{\Delta R}{R} = \alpha_R \cdot t + \beta_R \cdot Q \tag{18}$$

Parameter α determines the calendar aging and β the cycle aging, while subscript j represents either C or R, depending on whether it refers to cell capacity or to internal resistance, respectively. These four parameters are not constant, the calendar aging shows a linear dependence on the battery voltage and depends on the temperature modelled through an Arrhenius expression, as proposed in [43]. The cycle aging has a quadratic dependence on the mean voltage of the cycle (v_{cyc}), a linear relationship with the DOD and an exponential dependence on the current, which is modelled as in [44].

$$\alpha_j = a_{j,v} \cdot \left(v_c - a_{j,0}\right) \cdot e^{-\frac{a_{j,T}}{T}} \tag{19}$$

$$\beta_j = \beta_{j,v} \cdot \left(v_{cyc} - \beta_{j,v0}\right)^2 + \beta_{j,DOD} \cdot \Delta DOD + \beta_{j,I} \cdot e^{b_{\exp}\frac{|I|}{C}} + \beta_{j,0} \tag{20}$$

The parameters of these expressions are shown in Table 2. In the case of cycle aging, its parameters depend on the equivalent cycles of the battery, which therefore need to be obtained. The most common method to obtain the equivalent cycles (SOC_{equiv}) is the Rainflow Algorithm [45]. This algorithm makes it possible to obtain the SOC_{equiv} based on a state of charge cycle profile. A schematic diagram of the methodology applied is shown in Fig 8. The hourly power to be covered by the battery bank during a year of operation (D) and the electrical model serve to obtain the data required for the aging model, SOC, i_b, and battery bank voltage (v_b). The aging model makes it possible to obtain the loss of capacity and the increase in internal resistance and, therefore, the actual capacity (C_a) and the actual internal resistance (R_a). For the application of the model, a battery bank operating temperature that is constant and equal to 30ºC is considered.

	Parameter	ΔC	ΔR
Calendar	a_v	$2.716\ 10^5$	$9.486\ 10^3$
	a_0	3.1482 V	3.096 V
	a_T	6976 K	5986 K
Cycle	b_0	$2.71\ 10^{-5}$	$2.28\ 10^{-5}$
	b_v	$3.14\ 10^{-4}\ V^{-1}$	$3.208\ 10^{-4}\ V^{-1}$
	b_{v0}	3.683 V	3.741 V
	b_{DOD}	$1.61\ 10^{-6}$	$3.404\ 10^{-6}$
	b_I	$1.56\ 10^{-5}$	$1.56\ 10^{-5}$
	b_{exp}	1.8 h	1.8 h

Table 2. Aging model parameters.

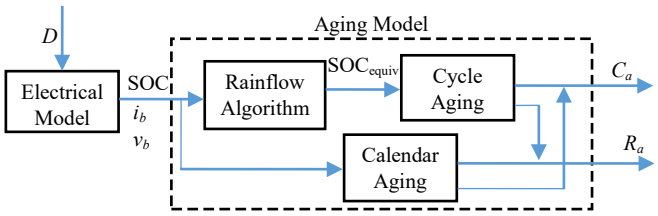

Fig. 8. Schematic diagram of aging model

The expected duration of the battery is set at ED = 10 years, and this involves applying the aging model for 10 years of operation, using the iterative process explained in subsection 2.2.3 For each year, there will be a reduction in capacity and an increase in internal resistance, involving a change in the evolution of the SOC and the assumed current, still demanding the same power profile from the battery bank. Thus, each year the internal resistance and capacity values are updated on the electrical model, making it possible to obtain the SOC, current (i_b) and voltage (v_b) of the battery bank, in other words, in Eqs. (13-16) the values of C and R obtained through the aging model, are updated. Finally, Eq. (12) is applied to obtain the number of batteries required (N_{c_AM}) for each value of f.

The result of this second stage of the sizing methodology is shown in Table 3, showing the maximum cumulative difference to be covered by the battery bank (DA_{max}), the number of batteries required to cover this difference N_{c_AM} and the energy available from the battery bank (E_b).

f	DA_{max} (kWh)	N_{c_AM}	E_b (kWh)
0	14.95	101	14.95
0.1	7.59	52	7.70
0.2	5.09	35	5.18
0.3	19.32	131	19.39
0.4	10.66	73	10.80
0.5	8.01	55	8.14
0.6	6.19	42	6.22
0.7	5.29	36	5.33
0.8	5.06	35	5.18
0.9	4.68	32	4.74
1	16.14	110	16.28

Table 3. Sizing of battery bank.

4 Results and discussion

4.1 Proposed solution

The results obtained with the proposed sizing methodology are shown in Section 3 for each of the 11 values of *f*. In order to select the best solution, the cost of each item in the installation is considered. The cost considered for the PV module was 162.6 € (2.2€ Wp^{-1}) [40], and, for the wind turbine, a cost of 1460 € (3.2€ W^{-1}) [39] and 74 € for the lithium-ion cell, this price implies a cost of 500€ kWh^{-1} [46].

Table 4 shows the cost of the stand-alone system obtained for each *f*. It can be seen that, from *f* is equal to 0, where the energy generated is sourced from the wind power subsystem, to *f* is equal to 0.2 the overall cost of the power supply subsystem decreases given the fact that the N_{c_AM} required decreases although the N_{PV} increases. For *f* is equal to 0.3 the cost increases despite the fact that N_W is equal to 1, due to the considerable increase in the N_{c_AM} required. As *f* increases, the N_{PV} increases until it reaches $f = 1$, where all the energy generated is sourced from the PV subsystem and, therefore, it considerably increases N_{c_AM}, given the fact that as N_W is zero, the complementarity existing between the wind power and PV resources is lost. Finally, based on the results shown, it is concluded that the optimum solution is between $f = 0.6$ and $f = 0.9$. The difference in costs between the said values for *f* is less than 2% of the solution with the lowest cost (5750.4 €), which is $f = 0.7$ and corresponds to 1 wind turbine, 10 PV modules and 36 batteries.

f	N_w	N_{pv}	N_{c_AM}	*Cost* (€)
0	3	0	101	11854
0.1	3	1	52	8390.64
0.2	3	2	35	7295.28
0.3	1	4	131	11804.56
0.4	1	6	73	7837.84
0.5	1	7	55	6668.48
0.6	1	8	42	5869.12
0.7	1	10	36	5750.40
0.8	1	11	35	5839.04
0.9	1	12	32	5779.68
1	0	13	110	10254.32

Table 4. Sizing of stand-alone TCS.

4.2 Comparison with other more conventional sizing methodologies

Normally, more conventional sizing methodologies do not consider the aging of the battery bank, the importance of which is decisive in order to guarantee the useful life of the stand-alone system. Moreover, when sizing the battery bank, many such methodologies consider a constant efficiency and do not take account of its electrical performance. This subsection makes an analysis of the differences existing between the proposed sizing methodology in relation to other more conventional methodologies. Specifically, for the case study, a comparison shall be made between the results obtained through the proposed sizing methodology and those obtained with a sizing considering a constant efficiency for the battery bank, and with another sizing that uses the electrical model to obtain the efficiency for each battery bank operating point. To do so, the algorithm proposed and shown in Fig. 1 shall be used to obtain the first case, sizing considering a constant efficiency of the battery bank, using the algorithm up to the first stage (pre-sizing). For this methodology, a battery bank efficiency of 95% is considered. For the second case, the sizing based on the electrical model to obtain the efficiency for each battery bank operating point, the algorithm shall be used up to the second stage (sizing by electrical model). For this method, the electrical model presented in subsection 3.2.5 is used.

Fig. 9 a, shows the N_c obtained in each sizing for each f. It can be seen that the N_c required when aging is taken into account, that is with the methodology proposed in this paper, is considerably greater than for the other sizing methodologies. Furthermore, it can be seen that, for all the values of f, the N_c required and obtained with the sizing by electrical model is greater than that obtained in the pre-sizing.

Fig. 9 b, shows the percentage relationship between the N_c obtained with the proposed sizing (sizing by aging model) and that obtained in the pre-sizing (N_{c_AM}/N_{c_P}) and the N_c obtained with the proposed sizing and that obtained with the electrical model (N_{c_AM}/N_{c_EM}). The differences with the pre-sizing are between 120 and 157% achieving the minimum value for $f = 0$ and the maximum for $f = 0.5$. With regard to the differences with the sizing by electrical model, these are lower and range between 109 and 117 %, for $f = 0.7$ and $f = 0.8$ respectively.

When performing the sizing, the influence of aging is considerable. In order to guarantee a continuous power supply to the loads, a greater N_c is required so that, for the entire expected useful life of the installation, the battery bank is capable of supplying the minimum power required. In this case, the expected duration must be considered to be equal to 10 years.

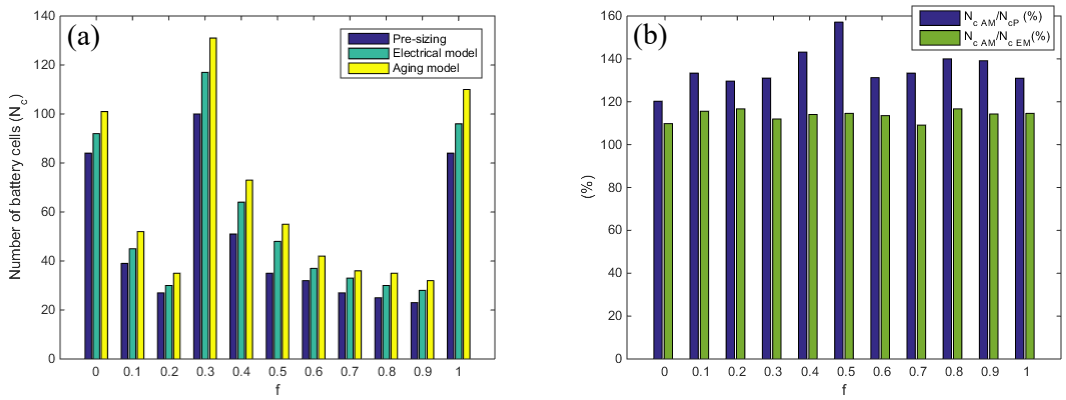

Fig. 9. a) Number of batteries (N_c) obtained for each sizing for each f and b) percentage relationship between the number of batteries obtained with the proposed sizing methodology and that obtained in the pre-sizing (N_{c_AM}/N_{c_P}) and that obtained in the sizing by electrical model (N_{c_AM}/N_{c_EM}) and for each f.

As is to be expected, taking aging into account, the energy needs increase over the years. This is due to the fact that the aging mechanisms cause the battery to lose capacity, with the subsequent loss of available energy, and to increase its internal resistance, thereby reducing the efficiency of the energy exchange.

On the other hand, it is worthy of note that the results obtained with the sizing by electrical model vary considerably in relation to those obtained in the pre-sizing. This highlights the importance of using the electrical model, given the fact that the pre-sizing would not achieve the energy required to ensure the continuous power supply to the loads for one year of system operation. The difference lies in the fact that the efficiency calculation to obtain the *DA* is made with the electrical model of the battery. This makes it possible to determine a sizing that is more suitable for the battery bank operating mode in the application in question. Fig. 10 shows N_{c_EM} obtained with the sizing by electrical model and the N_c obtained using a constant efficiency. The sizing was conducted with different mean efficiencies, from 0.8 to 0.98 with intervals of 0.02. The figure shows the battery minimum and maximum values obtained for the said efficiencies for each of the values for f. It can be seen that, for values for f that are greater than 0.2, the sizing with the electrical model gives an N_c value that is significantly different and, specifically, a greater number. The greatest difference is for $f = 0.5$ where 60% or 33% more cells are required in relation to the minimum and maximum values respectively, obtained using the mean and constant efficiency, than when using the electrical model.

The use of the electrical model for the sizing, makes it possible to obtain a solution that is more in line with the battery bank operating mode. Fig. 11 shows the variation in the efficiency obtained with the electrical model for $f = 0.2$. The said variation is completely related to the variation of the internal battery resistance with the SOC.

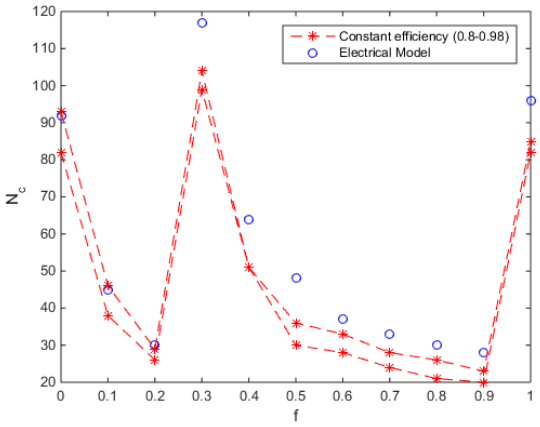

Fig. 10. Number of batteries (N_c) obtained with the sizing by electrical model and with the pre-sizing with constant efficiencies of 0.8 to 0.98 for each value of f.

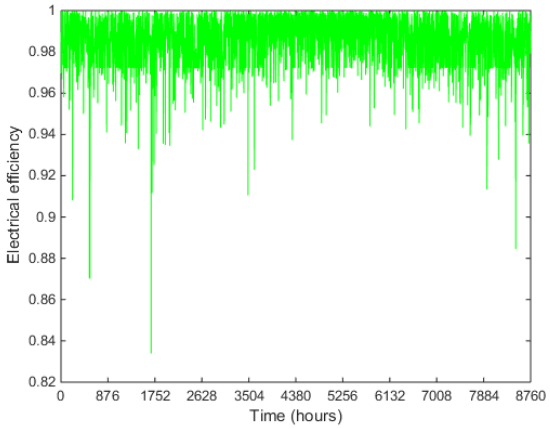

Fig. 11. Electrical efficiency for $f = 0.2$ during a year of operation of the stand-alone system.

Finally, an analysis was made of the cost of the installation in relation to each sizing methodology. Table 5 and Fig. 12 show the cost of the stand-alone system obtained for each sizing methodology (pre-sizing, sizing by electrical model and by aging model) for each value of f. It can be seen that, the optimum solution lies between $f = 0.6$ and $f = 0.9$ for the case of the pre-sizing and the sizing taking the electrical model into account, and between $f = 0.7$ and $f = 0.9$ for the case of the sizing taking aging into account. In the case of the pre-sizing, $f = 0.7$ is the least expensive solution for the system and corresponds to 1 wind turbine, 10 PV modules and 27 batteries. While, for the sizing with the electrical model, the least expensive solution is $f = 0.8$ and corresponds to 1 wind turbine, 11 PV modules and 30 batteries. For the sizing taking aging into account, as for the pre-sizing case, the least expensive solution is $f = 0.7$ with 36 batteries. It can be seen that, for the case study, the f corresponding to the optimum solution from a financial point of view, varies but slightly with regard to the sizing method used. Specifically, there is hardly any variation between the size of the renewable generation subsystem (N_w and N_{pv}) obtained for each sizing, yet the difference between the N_c according to the sizing methodology used, is extremely significant.

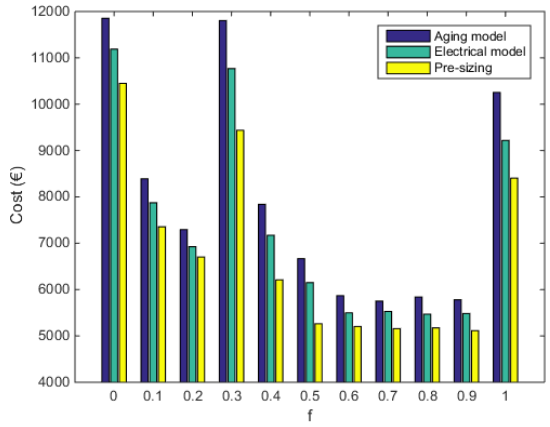

Fig. 12. Cost of the stand-alone system obtained for the pre-sizing, sizing by electrical model and with the proposed sizing (by aging model) for each value of *f*.

f	*Pre-sizing (€)*	*Electrical model (€)*	*Aging model (€)*
0	10596.00	11188.00	11854.00
0.1	7428.64	7872.64	8390.64
0.2	6703.28	6925.28	7295.28
0.3	9510.56	10768.56	11804.56
0.4	6209.84	7171.84	7837.84
0.5	5188.48	6150.48	6668.48
0.6	5129.12	5499.12	5869.12
0.7	5084.40	5528.40	5750.40
0.8	5099.04	5469.04	5839.04
0.9	5113.68	5483.68	5779.68
1	8330.32	9218.32	10254.32

Table 5. Cost of the stand-alone system obtained for the pre-sizing, sizing by electrical model and with the proposed sizing (by aging model) for each value of *f*.

5 Conclusions

This paper proposes a methodology for the sizing of stand-alone hybrid solar PV-wind systems. This methodology makes it possible to optimise the sizing of the components of the stand-alone system, based on the premise of guaranteeing the power supply to the loads throughout the useful life of the installation at a minimum cost. The sizing is performed in two stages. Firstly, the components of the wind and PV power generation system are obtained and, secondly, the size of the storage subsystem is calculated. For the storage subsystem sizing, account is taken of the variation in efficiency in relation to the operating point of the subsystem and also the

deterioration of the subsystem due to aging and, therefore, the loss of available energy during the useful life of the installation. The sizing methodology results in 11 potential solutions that guarantee the continuous supply of electricity to the load for the useful life of the installation. Each of these 11 potential solutions has an associated financial cost. The optimum solution is the one involving the lowest cost for the stand-alone system.

This methodology is applied to an actual system, specifically to a TCS located on a secondary road. For this purpose, a detailed study was made of the TCS loads, achieving a considerable reduction in the consumption, which can be extrapolated to other systems that are intended to be connected to the grid and where priority has been given to functionality over power consumption. The measures adopted, have led to a reduction in the cost of the subsequently designed renewable power supply stand-alone system. Secondly, the sizing methodology was applied, resulting in a hybrid wind power - PV generation subsystem with a storage subsystem based on lithium-ion batteries

Finally, an analysis was made of the proposed methodology, and the results obtained were compared with other more conventional sizing methodologies, specifically by sizing the battery bank solely based on mean and constant efficiency, the energy capacity obtained may not be sufficient to guarantee the power supply. This is due to the fact that efficiency varies in relation to the state of charge and, depending on the operating mode, efficiency changes considerably. Conversely, when the sizing was made with the electrical model, a variable efficiency was obtained, as a function of the battery bank operating point. This guarantees that the energy capacity ensures a continuous power supply to the loads. Moreover, the battery aging implies a reduction in its capacity and, therefore, a reduction in the battery power capacity and an increase in its internal resistance, resulting in a reduction in energy conversion performance. Therefore, if the battery bank aging is taken into account, it is possible to guarantee the power supply over the useful life of the system, with no need to replace, a priori, the battery bank.

Although in the case study the use of lithium-ion batteries are proposed, these can be replaced by other storage systems, such as systems based on hydrogen with supercapacitors, or other battery technologies, given the fact that the proposed sizing methodology can be applied irrespective of the storage technology used.

Acknowledgements

This work has been supported by the Spanish State Research Agency (AEI) and FEDER-UE under grant DPI2013-42853-R, DPI2016-80642-R and DPI2016-80641-R; and by the Government of Navarre under project PIO38 INTEGRA-RENOVABLES.

References

[1] Zhou W, Lou C, Li Z, Lu L, Yang H. Current status of research on optimum sizing of stand-alone hybrid solar–wind power generation systems. Appl Energy 2010;87:380–9.

[2] Bajpai P, Dash V. Hybrid renewable energy systems for power generation in stand-alone applications: A review. Renew Sustain Energy Rev 2012;16:2926–39.

[3] Bernal-Agustín J.L, Dufo-López R. Simulation and optimization of stand-alone hybrid renewable energy systems. Renew Sustain Energy Rev 2009;13:2111–8.

[4] Ursúa A, San Martín I, Barrios E L, Sanchis P. Stand-alone operation of an alkaline water electrolyser fed by wind and photovoltaic systems. Int J Hydrogen Energy, 2013;38 (35), pp. 14952-67.

[5] Ursúa A, Barrios EL, Pascual J, San Martín I, Sanchis P. Integration of commercial alkaline water electrolysers with renewable energies: Limitations and improvements. Int J Hydrogen Energy 2016;41(30):12852-61.

[6] San Martín I, Ursúa A, Sanchis P. Modelling of PEM fuel cell performance: Steady-state and dynamic experimental validation. Energies 2014;7(2):670-700.

[7] Ursúa A, Sanchis P. Static-dynamic modelling of the electrical behaviour of a commercial advanced alkaline water electrolyser. Int J Hydrogen Energy 2012;37(24):18598-614.

[8] San Martín I, Ursúa A, Sanchis P. Integration of fuel cells and supercapacitors in electrical microgrids: Analysis, modelling and experimental validation. Int J Hydrogen Energy 2013;38(27):11655-71.

[9] Berrueta A, San Martín I, Hernández A, Ursúa A, Sanchis P. Electro-thermal modelling of a supercapacitor and experimental validation. J Power Sources 2014;259:154-65.

[10] Olabi A G. Renewable energy and energy storage systems. Energy 2017; 136:1-6

[11] Chen H, Cong TN, Yang W, Tan C, Li Y, Ding Y. Progress in electrical energy storage system: A critical review. Prog Nat Sci 2009;19:291–312.

[12] Kousksou T, Bruel P, Jamil A, El Rhafiki T, Zeraouli Y. Energy storage: Applications and challenges. Sol Energy Mater Sol Cells 2014;120:59–80.

[13] Ma T, Yang H, Lu L. Performance evaluation of a stand-alone photovoltaic system on an isolated island in Hong Kong. Appl Energy 2013;112:663–72.

[14] Kaldellis JK. Optimum hybrid photovoltaic-based solution for remote telecommunication stations. Renew Energy 2010;35:2307–15.

[15] Ekren O, Ekren BY, Ozerdem B. Break-even analysis and size optimization of a PV/wind hybrid energy conversion system with battery storage – A case study. Appl Energy 2009;86:1043–54.

[16] Ekren BY, Ekren O. Simulation based size optimization of a PV/wind hybrid energy conversion system with battery storage under various load and auxiliary energy conditions. Appl Energy 2009;86:1387–94.

[17] Ma T, Yang H, Lu L. A feasibility study of a stand-alone hybrid solar–wind–battery system for a remote island. Appl Energy 2014;121:149–58.

[18] Diouf B, Pode R. Potential of lithium-ion batteries in renewable energy. Renew Energy 2014; 76:375-80.

[19] Khare V., Nema S., Baredar P. Solar–wind hybrid renewable energy system: A review. Renew Sustain Energy Rev 2016; 58: 23-33.

[20] Nema P, Nema RK, Rangnekar S. A current and future state of art development of hybrid energy system using wind and PV-solar: A review. Renew Sustain Energy Rev 2009;13:2096–103.

[21] Erdinc O, Uzunoglu M. Optimum design of hybrid renewable energy systems: Overview of different approaches. Renew Sustain Energy Rev 2012;16:1412–25.

[22] Chen H-C. Optimum capacity determination of stand-alone hybrid generation system considering cost and reliability. Appl Energy 2013;103:155–64.

[23] Connolly D, Lund H, Mathiesen BV, Leahy M. A review of computer tools for analysing the integration of renewable energy into various energy systems. Appl Energy 2010;87:1059–82.

[24] Luna-Rubio R, Trejo-Perea M, Vargas-Vázquez D, Ríos-Moreno GJ. Optimal sizing of renewable hybrids energy systems: A review of methodologies. Sol Energy 2012;86:1077–88.

[25] Ahadi A., Kang S–K., Lee J-H. A novel approach for optimal combinations of wind, PV, and energy storage system in diesel-free isolated communities. Appl Energy 2016;15:101–15.

[26] Li D, Danilov D L, Xie J, Raijmakers L, Gao L, Yang Y, Notten P H L. Degradation Mechanisms of C6/LiFePO4 Batteries: Experimental Analyses of Calendar Aging. Electroch. Acta 2016;190:1124-33.

[27] http://www.meteosim.com/ ; 2017

[28] Kazimierczuk M K. Pulse-Width Modulated DC-DC Power Converters. Chichester, UK: John Wiley & Sons, Ltd; 2016.

[29] http://eosweb.larc.nasa.gov/sse/ ; 2017

[30] http://re.jrc.ec.europa.eu/pvgis/; 2017

[31] http://www.meteonorm.com/; 2017

[32] Luque A. HS. Handbook of Photovoltaic Science and Engineering. Chichester, UK: John Wiley & Sons, Ltd; 2003.

[33] Lorenzo E. Solar Electricity: Engineering of Photovoltaic Systems. Madrid, Spain: Progensa; 1994.

[34] Moriana I, San Martin I, Sanchis P. Wind-photovoltaic hybrid systems design. SPEEDAM 2010, IEEE; 2010, p. 610–5.

[35] http://www.dgt.es/es/seguridad-vial/unidad-de-victimas-de-accidentes-de-trafico; 2017

[36] Vaa T, Penttinen M, Spyropoulou I. Intelligent transport systems and effects on road traffic accidents: state of the art. IET Intell Transp Syst 2007;1:81.

[37] Cheng HH. A Review of the Applications of Agent Technology in Traffic and Transportation Systems. IEEE Trans Intell Transp Syst 2010;11:485–97.

[38] http://www.cit.gva.es/cast/carreteras/aforos-car/informes-anuales-car/ ; 2017

[39] http://www.silentwindgenerator.com; 2017

[40] http://www.ennovaenergia.com ; 2017

[41] Berrueta A, Urtasun A, Ursúa A, Sanchis P. A comprehensive model for lithium-ion batteries: From the physical principles to an electrical model. Energy 2018;144:286-300.

[42] Berrueta A., Irigaray V., Sanchis P., Ursúa A. Lithium-ion battery model and experimental validation. 17th Eur. Conf. Power Electron. Appl. (EPE'15 ECCE-Europe), IEEE; 2015, 1–8.

[43] Schmalstieg J., Käbitz S., Ecker M., Sauer D. U. From accelerated aging tests to a lifetime prediction model: Analyzing lithium-ion batteries. World Electr. Veh. Symp. Exhib., IEEE; 2013; 1–12.

[44] Wang J., Purewal J., Liu P., Hicks-Garner J., Soukazian S., Sherman E., Sorenson A., Vu L., Tataria H., Verbrugge M. W. Degradation of lithium ion batteries employing graphite negatives and nickel-cobalt-manganese oxide + spinel manganese oxide positives: Part 1, aging mechanisms and life estimation. J Power Sources, 269:937-948, 2014.

[45] Musallam M., Johnson, C. M. An Efficient Implementation of the Rainflow Counting Algorithm for Life Consumption Estimation. IEEE Trans Reliab 2012;61:978–86.

[46] https://www.tesla.com; 2017